Available online at www.sciencedirect.com
SCIENCE DIRECT
Thermochimica Acta 444 (2006) 35–45
thermochimica acta
www.elsevier.com/locate/tca

Decomposition of tetra-alkylammonium thiomolybdates characterised by thermoanalysis and mass spectrometry

M. Poisot [a], W. Bensch [a,*], S. Fuentes [b], G. Alonso [c]

[a] *Institut für Anorganische Chemie, University of Kiel, Olshausenstr. 40-60, 24118 Kiel, Germany*
[b] *Centro de Ciencias de la Materia Condensada, Universidad Nacional Autonoma de, Mexico, Apdo. Postal 2681, Ensenada, Baja California, CP 22800, Mexico*
[c] *Centro de Investigación en Materiales Avanzados, Miguel de Cervantes No. 120, Chihuahua, Chih., CP 31110, Mexico*

Received 22 November 2005; received in revised form 24 January 2006; accepted 21 February 2006
Available online 28 February 2006

Abstract

The decomposition pattern of tetraalkyl-tetrathiomolybdates with general formula $(R_4N)_2MoS_4$ (with R increasing from methyl to heptyl) was determined by means of differential thermal analysis (DTA), thermogravimetric analysis (TGA) and mass spectroscopy (MS) techniques. The complexity of thermal decomposition reactions increases with the size of the R_4N group. Prior to decomposition at least one phase transition seems to occur in all complexes. The onset of thermal reactions was also a function of the tetra-alkylammonium precursor. All compounds decompose without forming sulfur rich MoS_{2+x} intermediates. For R = methyl to pentyl precursors the MoS_2 produced was nearly stoichiometric, however for R = hexyl and heptyl the S content was significantly reduced with a Mo:S ratio of about 1.5. The carbon and hydrogen residual contents in the product increased with the number of C atoms in R_4N; for N contamination no clear trend was obvious. SEM images show that the formation of macro-pores was also a function of the alkyl group in R_4N. The MoS_2 materials obtained show a sponge-like morphology. Results of DSC experiments in combination with in situ X-ray diffraction also revealed the complex thermal behavior of $(R_4N)_2MoS_4$ materials; reversible and irreversible phase transitions and glass-like transformations were identified in the low temperature range (35–140 °C), before the onset of decomposition.

Keywords: Thiometallates; Tetraalkyl-thiomolybdates; MoS_2 preparation; Thermal decomposition; Thermoanalysis

1. Introduction

Transition metal thiometallate complexes are useful for applications in several processes as biological [1], enzymatic [2] and as catalyst precursors [1,3–9]. Preparation of catalysts with better catalytic activity and stability than the present ones represents a great challenge for the industry and implies the search of new routes of preparation. During the last few years a number of contributions appeared in the literature dealing with different approaches to synthesize MoS_2 catalysts under different synthetic conditions and also the use of alkylthiometallates as catalysts precursors have been reported [10–21]. Transition metal sulfides (TMS), particularly molybdenum and tungsten sulfides, promoted with Co or Ni and supported on alumina are typically used in hydrotreating reactions [22]. The use of bis-thiometallates containing Co, Ni and Mo as precursors of hydrotreating catalysts has been reported [23–26].

The decomposition of ammonium thiomolybdate (ATM) and ammonium thiotungstate (ATT) has been studied by several authors [27,28].

More recently it has been studied by X-ray absorption fine structure spectroscopy (EXAFS) and powder X-ray diffraction (XRD) [29–31]. These compounds form trisulfide compounds $Mo(W)S_3$ as intermediates prior to be transformed to the poorly crystalline (pc) form of MoS_2. The decomposition of tetra-alkylammonium thiometallates has been used for preparation of MoS_2 catalysts for hydrodesulfurization and has been analyzed by means of DTA and TG [32] however a clear mechanism of the process has not yet been reported.

In this work, a further study of tetra-alkylammonium thiomolybdates decomposition patterns by means of combined techniques DTA–TG–DTG and MS is performed. The main goal in this work is to provide a general picture of the decom-

* Corresponding author. Tel.: +49 431 880 2091.
E-mail address: wbensch@ac.uni-kiel.de (W. Bensch).

0040-6031/$ – see front matter © 2006 Elsevier B.V. All rights reserved.
doi:10.1016/j.tca.2006.02.025

position process of tetra-alkyl thiomolybdates $(R_4N)_2MoS_4$, where R changes from C1 (methyl) up to C7 (heptyl).

2. Experimental

2.1. Preparation of $(R_4N)_2MoS_4$ precursors

The synthesis of the tetra-alkylammonium salts $(R_4N)_2MoS_4$ has been reported by McDonald et al. [33]. Later this method was improved by Alonso et al. [34]. In the present work, a modified version of the last method was used.

2.1.1. Synthesis of tetramethyl-, tetraethyl-, tetrapropyl-ammonium thiomolybdate

Fresh prepared $(NH_4)_2MoS_4$ (5 mmol) was dissolved in water (30 ml) and stirred. $(R)_4NBr$ (10 mmol) was dissolved in a solution of NaOH (10 mmol) in 30 ml water and stirred. The first solution was added to the second and the mixture was stirred for 30 min. The solution was kept undisturbed over ice and after one night red crystals precipitated. The solid was filtered and washed with cold water and ethanol, the yield was 80%. These compounds are stable in air for a long time.

2.1.2. Synthesis of tetrabutyl-, tetrapentyl-, tetrahexyl-, and tetraheptyl-ammonium thiomolybdates

Fresh synthesized $(NH_4)_2MoS_4$ (1.9 mmol) was dissolved in water (10 ml) and stirred until a clear solution was obtained. To this solution an aqueous solution of $(R)_4NBr$, R = butyl, pentyl, (3.8 mmol, 20–25 ml water) was added and the mixture was stirred for 30 min. For R = hexyl and heptyl the synthesis was performed in methanol. First a gel-like solid was formed and after ethanol was added dark red crystals precipitated. The solid was filtered and washed with cold water, and the yield was 90%. These compounds are unstable in air and they were stored under nitrogen atmosphere.

2.2. Methods and materials

A CHN-O RAPID combustion analyzer from Heraeus was used to determine the chemical composition of the materials. The samples were heated up to 1000 °C under an oxygen atmosphere in zinc sample holders and the gases were then detected by gas chromatography.

A Philips ESEM XL 30 microscope equipped with an EDAX analyzer was used to perform morphological and elemental analysis. Pictures were taken at different areas of the samples applying different magnifications.

DTA–TG–MS measurements were undertaken simultaneously using a STA-409CD with Skimmer coupling from Netzsch, which is equipped with a quadrupole mass spectrometer QMA 400 (maximum 512 amu) from Balzers. The MS measurements were performed in analog and trend scans modes. All TG curves were corrected for buoyancy and current effects. The heating rate was 4 K/min up to 350 °C. For DTA–TG experiments the samples were placed in Al_2O_3 crucibles under a dynamic nitrogen atmosphere (flow rate: 75 ml/min, purity 5.0). DTA–TG–MS measurements were performed under a dynamic helium atmosphere (flow rate: 50 ml/min, purity 5.6). The MS spectra recorded were compared with data from the National Institute of Standards and Technology, NIST (http://webbook.nist.gov/chemistry). DSC experiments (heating rate: 3 K/min; final temperature: 150 °C) were performed with

Table 1
Data of chemical analysis, weight loss and thermal events for $(R_4N)_2MoS_4$

R	Weight loss (%)	C (%)	H (%)	N (%)	S (%)	Composition	T_p (°C)	T_{onset} (°C)
Methyl	−56.5	25.9	6.5	7.5	34.5	$MoS_{1.96}C_{0.2}N_{0.02}$	246	239
		25.8	6.49	7.52	34.43			
		1.5	0.0	0.2	39			
Ethyl	−64	39.3	8.2	5.7	26.1	$MoS_{1.96}C_{0.79}N_{0.04}H_{0.5}$	43, 224	40, 217
		39.65	8.32	5.78	26.46			
		5.6	0.3	0.4	37.1			
Propyl	−71.4	47.9	9.4	4.6	20.9	$MoS_{1.97}C_{0.73}N_{0.04}H_{0.5}$	108, 176, 222	102, 169, 216
		48.29	9.46	4.69	21.49			
		5.2	0.3	0.4	37.4			
Butyl	−74	54.0	10.1	3.9	18.1	$MoS_{2.03}C_{1.13}N_{0.04}H_{0.8}$	117, 142, 167, 194	115, 139, 157, 189
		54.2	10.23	3.95	18.09			
		7.7	0.5	0.4	37			
Pentyl	−76	58.2	10.6	3.3	15.4	$MoS_{1.99}C_{1.18}N_{0.07}H_{1.14}$	218	205
		58.49	10.8	3.41	15.62			
		8.1	0.6	0.5	36.3			
Hexyl	−79.6	61.5	11.1	3.0	13.4	$MoS_{1.5}C_{1.53}N_{0.09}H_{2.14}$	167, 239, 292	162, 212
		61.76	11.23	3.0	13.74			
		11.1	1.3	0.8	29.1			
Heptyl	−81	64.2	11.7	2.7	11.9	$MoS_{1.3}C_{2.6}N_{0.13}H_{3.33}$	76, 178, 275	72, 158, 244
		64.32	11.57	2.68	12.26			
		18.1	1.9	1.1	24.3			

Chemical composition: first line, experimental values; second line, theoretical values; third line, after decomposition.

a Netzsch DSC 204 Phoenix instrument using aluminum crucibles covered with aluminum lid. Sealed glass ampoules filled with argon were also used as sample carriers to prevent a reaction of the samples with Al. The ampoules were mounted in an aluminum shoe to ensure a good thermal contact with the thermocouple. An empty sealed glass ampoule with an Al shoe was used as reference. For these experiments just the temperature was calibrated measuring mercury, indium, tin and bismuth provided by Netzsch.

3. Results

3.1. Elemental analysis

The results of chemical analysis of the MoS_2 catalysts before and after the thermal decomposition of tetra-alkyl thiomolybdate precursors are shown in Table 1. The content of carbon in the decomposed products increases gradually with the size of the alkyl group, from 1.5 wt.% for tetramethylammonium up to 18.1 wt.% for tetraheptylammonium. The amount of hydrogen and nitrogen also increase from tetramethylammonium to tetraheptylammonium tetrathiomolybdate (from 0 to 1.9 wt.% for H and from 0.2 to 1.1 wt.% for N). According to the chemical analyses the atomic ratio S/Mo is about 2 for the precursors with R = methyl until R = pentyl. But for the hexyl and heptyl samples the S concentration is significantly lower. The atomic composition of the catalysts in Table 1 shows that carbon and hydrogen coexist with MoS_2 in about the same proportion for catalysts derived from C1 to C5 alkyl groups suggesting that they may exist combined as CH groups which remain trapped between the MoS_2 layers or adsorbed on its surface. Otherwise, the amount of N is much lower than that of C and H and are considered as residual trace. The composition of catalysts formed from C6 and C7 alkyl precursors show an important reduction of S concentration as well as a significant augment of C and H, suggesting that these elements substituted partially S in the structure of MoS_2.

These results clearly indicate that the size of alkyl precursor influence the final composition of the decomposition products and that carbon and hydrogen can be an important part of the final MoS_2 catalyst.

3.2. DTA–TG–DTG–MS characterization

3.2.1. Tetramethylammonium thiomolybdate $((CH_3)_4N)_2MoS_4$

The thermal decomposition reaction of $((CH_3)_4N)_2MoS_4$ occurred in one step starting at about 240 °C, accompanied by a strong endothermic peak at T_{onset} = 239 °C (Fig. 1). During this event a mass loss of 56.5% was detected. The weight loss process ended at 350 °C. The thermal decomposition reaction can be represented as

$$((CH_3)_4N)_2MoS_4 \rightarrow 2(CH_3)_3N + (CH_3)_2S_2 + MoS_{1.96}C_{0.2}N_{0.02} \quad (1)$$

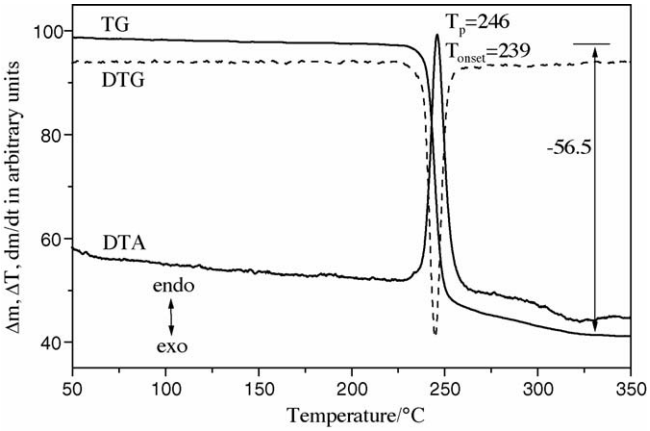

Fig. 1. DTA, TG and DTG plot of $[(methyl)_4N]_2[MoS_4]$ decomposition. Temperature in °C and weight loss in %.

The theoretical mass loss expected for the formation of MoS_2 is 57%, and therefore it can be assumed that some amount of carbon remained trapped or adsorbed in MoS_2. The mass spectrum (Fig. 2) shows that trimethylamine (m/z = 59) and dimethyldisulfide (m/z = 94) were emitted at 240 °C, it is related to the endothermic peak detected. The TG–MS results indicate that tetramethylammonium thiomolybdate decomposes at lower temperature than ammonium thiomolybdate (ATM) and also as shown in Eq. (1) it does not form MoS_3 as an intermediate which further decomposes to MoS_2 as ATM typically does [28,35–38].

3.2.2. Tetraethylammonium thiomolybdate $((CH_3CH_2)_4N)_2MoS_4$

The thermal decomposition reaction of $((CH_3CH_2)_4N)_2MoS_4$ also took place in one step starting at 200 °C, however it was accompanied by at least two endothermic peaks (Fig. 3). The nature of the event at low temperature (T_{onset} = 40 °C) was analyzed by DSC and XRD and will be discussed below. The second peak (T_{onset} = 217 °C) can be assigned to the amine fragmentation and elimination. Similarly to the methyl precursor endothermic peaks may be attributed to molecule rearrangement and formation of diethyldisulfide (DEDS).

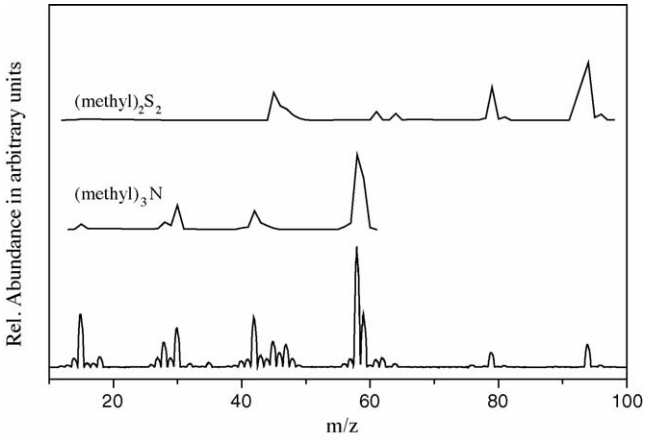

Fig. 2. Mass spectrum of $[(methyl)_4N]_2[MoS_4]$ decomposition at 240 °C. *Note*: the top two traces were taken from http://webbook.nist.gov/chemistry.

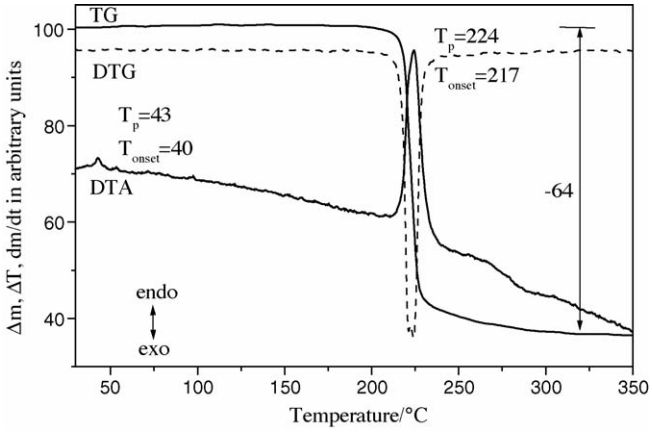

Fig. 3. DTA, TG and DTG plot of $[(ethyl)_4N]_2[MoS_4]$ decomposition. Temperature in °C and weight loss in %.

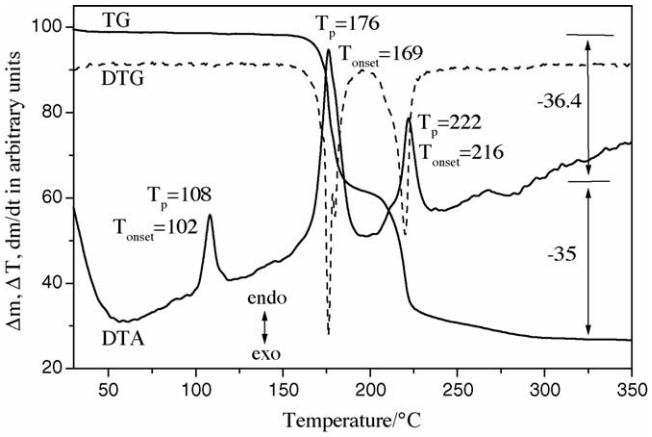

Fig. 5. DTA, TG and DTG plot of $[(propyl)_4N]_2[MoS_4]$ decomposition. Temperature in °C and weight loss in %.

The experimental weight loss of 64.2% is lower than the theoretical value of 66.95% for the formation of MoS_2, in agreement with the larger amount of residual carbon than in the methyl precursor (see Table 1). The weight loss also ended at 350 °C. The corresponding equation is

$$((CH_3CH_2)_4N)_2MoS_4 \rightarrow 2(CH_3CH_2)_3N + (CH_3CH_2)_2S_2 + MoS_{1.96}C_{0.79}N_{0.04}H_{0.5} \quad (2)$$

The MS spectrum (Fig. 4) shows the emission of triethylamine ($m/z = 101$) and DEDS ($m/z = 122.16$) which indicates that a similar pattern of fragmentation as in the methyl precursor occurred, indeed the onset of decomposition decreased to 200 °C. Again, there are no hints for the formation of MoS_3 as an intermediate.

3.2.3. Tetrapropylammonium thiomolybdate $((CH_3(CH_2)_2)_4N)_2MoS_4$

The thermal decomposition reaction of this precursor is more complex than in the previous cases and a two-step decomposition mechanism starting at about 155 and 210 °C is observed (Fig. 5). The first strong endothermic peak at $T_{onset} = 102$ °C corresponds to a phase transition of the crystal structure, whereas the other endothermic events at $T_{onset} = 169$ and 216 °C may be due to molecular redistribution and fragmentation. In the first decomposition step the weight loss amounts to 36.4% while during the next thermal process the weight loss is 35%. The experimental weight change is again lower than the expected value of 73.1% for the formation of MoS_2, and the thermal reaction path may be formulated as

$$((CH_3(CH_2)_2)_4N)_2MoS_4 \rightarrow 2(CH_3(CH_2)_2)_3N + (CH_3(CH_2)_2)_2S_2 + MoS_{1.97}C_{0.73}N_{0.04}H_{0.5} \quad (3)$$

From this equation a substantial increase in retained carbon is observed, but the S content remains very close to stoichiometric values. The weight loss ends at 300 °C, lower than for the two previous samples.

In the mass spectrum (Fig. 6) tripropylamine ($m/z = 143$) and dipropyldisulfide ($m/z = 150$) are identified in both decomposition steps. Both compounds are released at temperatures where the endothermic peak occurs in the DTA trace.

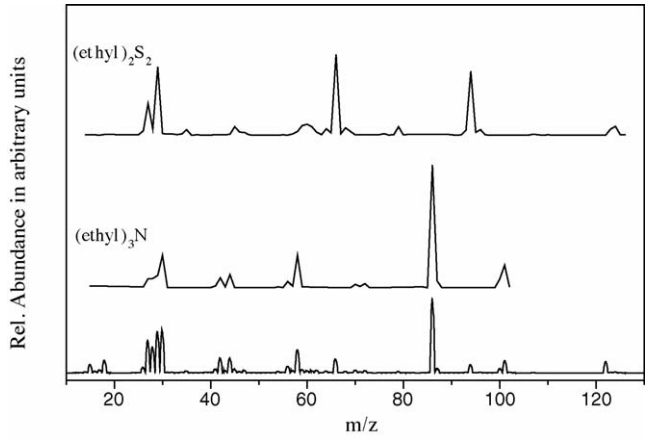

Fig. 4. Mass spectrum of $[(ethyl)_4N]_2[MoS_4]$ decomposition at 222 °C. *Note*: the top two traces were taken from http://webbook.nist.gov/chemistry.

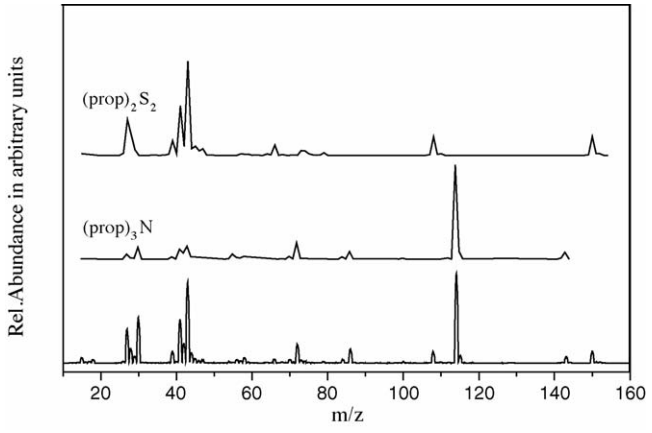

Fig. 6. Mass spectrum of $[(propyl)_4N]_2[MoS_4]$ decomposition at 175 °C. *Note*: the top two traces were taken from http://webbook.nist.gov/chemistry.

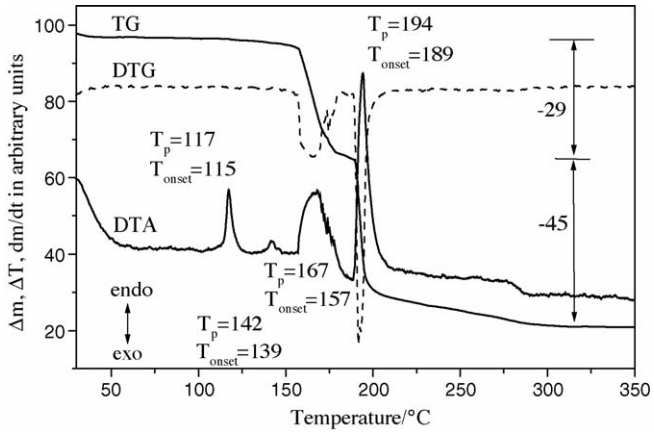

Fig. 7. DTA, TG and DTG plot of $[(butyl)_4N]_2[MoS_4]$ decomposition. Temperature in °C and weight loss in %.

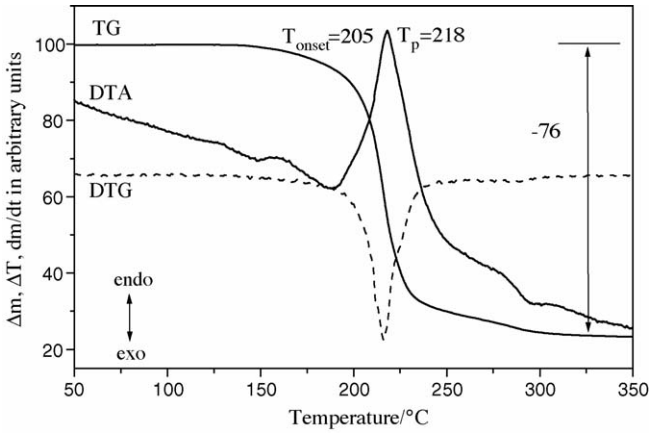

Fig. 9. DTA, TG and DTG plot of $[(pentyl)_4N]_2[MoS_4]$ decomposition. Temperature in °C and weight loss in %.

3.2.4. Tetrabutylammonium thiomolybdate $((CH_3(CH_2)_3)_4N)_2MoS_4$

The thermal decomposition reaction of tetrabutylammonium thiomolybdate is also complex (Fig. 7). First a phase transition (endothermic) occurs at $T_{onset} = 115\,°C$. The second ($T_{onset} = 139\,°C$) and third events ($T_{onset} = 157\,°C$) are accompanied by a weight loss of 29%. During the fourth endothermic peak at $T_{onset} = 189\,°C$ a mass change of 45% is observed. The total weight loss (74%) is again lower than the theoretical value for MoS_2 formation (77.2%), and the thermal decomposition reaction may be formulated as

$$((CH_3(CH_2)_3)_4N)_2MoS_4 \rightarrow 2(CH_3(CH_2)_3)_3N + (CH_3(CH_2)_3)_2S_2 + MoS_{2.03}C_{1.13}N_{0.04}H_{0.8} \quad (4)$$

The large amount of residual carbon in this sample indicates that the elimination of organic fractions from MoS_2 was not very efficient. The two decomposition steps starting at 160 and 190 °C took place at temperatures slightly lower than those in the tetrapropylammonium sample. Similar to the previous case the weight loss ended at 300 °C. Analysis of MS data (Fig. 8) suggests that tributylamine ($m/z = 185$) and dibutyldisulfide ($m/z = 178$) were released during both weight loss steps.

3.2.5. Tetrapentylammonium thiomolybdate $((CH_3(CH_2)_4)_4N)_2MoS_4$

In the DTA curve of the thermal decomposition of $((CH_3(CH_2)_4)_4N)_2MoS_4$ no events indicative for a phase transition are seen. A continuous decay with a broad and strong signal at $T_{onset} = 205\,°C$ occurs in the DTA curve. The TG trace (Fig. 9) shows that degradation of the sample starts at about 150 °C and is accompanied by a total mass loss of 76%, significantly lower than the calculated value (80.3%) for MoS_2 formation. The weight loss ended at 300 °C.

According to the mass spectrometry results (emission of tripentylamine ($m/z = 227$) and dipentyldisulfide ($m/z = 206$) (Fig. 10)) and the chemical analysis of the final product the thermal decomposition reaction of the material may be represented by the equation:

$$((CH_3(CH_2)_4)_4N)_2MoS_4 \rightarrow 2(CH_3(CH_2)_4)_3N + (CH_3(CH_2)_4)_2S_2 + MoS_{1.99}C_{1.18}N_{0.07}H_{1.14} \quad (5)$$

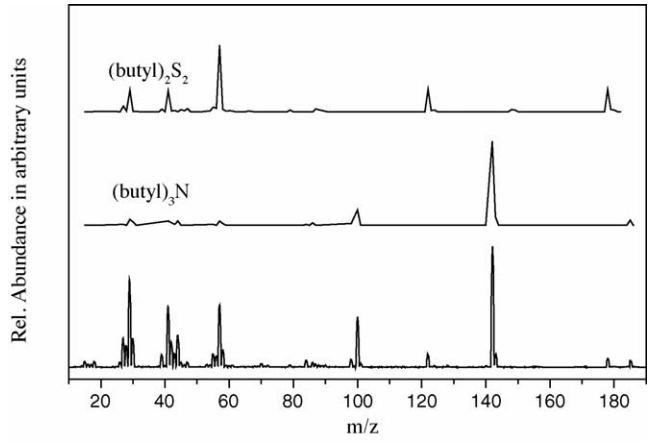

Fig. 8. Mass spectrum of $[(butyl)_4N]_2[MoS_4]$ decomposition at 196 °C. *Note*: the top two traces were taken from http://webbook.nist.gov/chemistry.

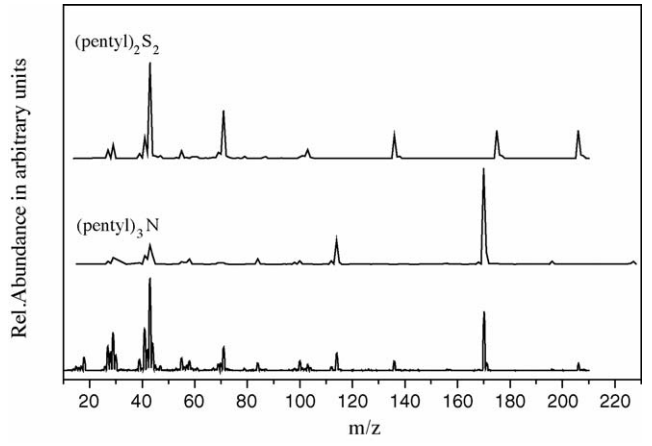

Fig. 10. Mass spectrum of $[(pentyl)_4N]_2[MoS_4]$ decomposition at 218 °C. *Note*: the top two traces were taken from http://webbook.nist.gov/chemistry.

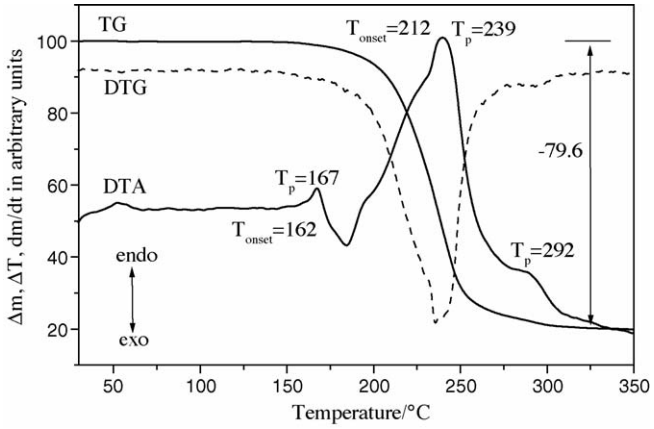

Fig. 11. DTA, TG and DTG plot of $[(hexyl)_4N]_2[MoS_4]$ decomposition. Temperature in °C and weight loss in %.

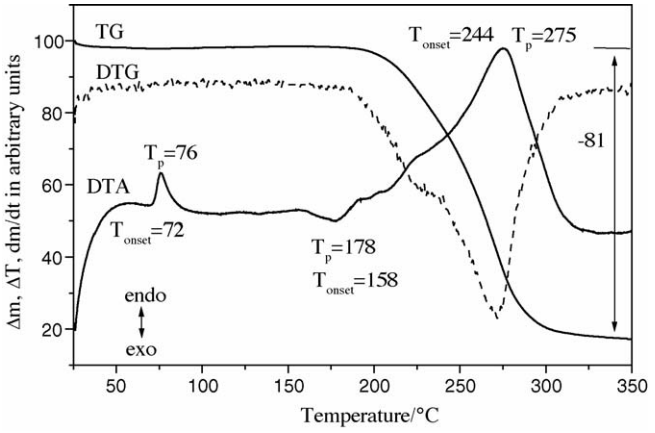

Fig. 13. DTA, TG and DTG plot of $[(heptyl)_4N]_2[MoS_4]$ decomposition. Temperature in °C and weight loss in %.

3.2.6. Tetrahexylammonium thiomolybdate $((CH_3(CH_2)_5)_4N)_2MoS_4$

This compound decomposed in a broad single step from about 180 to 330 °C. The DTA signal shows three peaks at T_{onset} = 162, 212 °C, and at T_p = 292 °C (Fig. 11). The origin of the first peak is not clear, but the signal may be due to melting of the material. In the DSC experiments (see below) a glass-like transition is seen and the product was more compact after a heat treatment up to 150 °C. Directly after the endothermic signal at T_{onset} = 162 °C an exothermic event occurs and the thermal degradation started immediately after this event. The rest of the broad and more or less featureless endothermic peaks correspond to the single weight loss of 79.6%. The difference to the theoretical value for MoS_2 formation of 82.6% is explained by the chemical analysis giving as composition $MoS_{1.5}C_{1.53}N_{0.09}H_{2.14}$. Obviously, during the thermal reaction a large fraction of S is emitted whereas C, H and N are retained in the sample. In the MS curves (Fig. 12) signals of trihexylamine (m/z = 269) and dihexyldisulfide (m/z = 234.2) are detected. According to these results the thermal decomposition reaction may be formulated as for the other precursors.

3.2.7. Tetraheptylammonium thiomolybdate $((CH_3(CH_2)_6)_4N)_2MoS_4$

The thermal decomposition reaction of tetraheptylammonium thiomolybdate is displayed in Fig. 13. The TG and DTG curves show that the decomposition covers a large temperature range from 180 to 350 °C. In the DTA trace one event occurs at T_{onset} = 72 °C that may be associated with a phase transition. This phenomenon will be further discussed below in the DSC and in situ X-ray scattering section. The small exothermic event at T_{onset} = 158 °C may be due to a rearrangement of the structure immediately before the decomposition starts; and the stronger endothermic peak at 244 °C is associated with the weight loss of 81%. The DTA signal is very broad indicating a complex fragmentation and reorganization of the constituents in the compound. The theoretical value for MoS_2 formation is 84.5%, and the difference is explained on the basis of chemical analysis of the final product yielding as composition $MoS_{1.3}C_{2.6}N_{0.13}H_{3.3}$. Like for $((CH_3(CH_2)_5)_4N)_2MoS_4$ a large amount of S is emitted during the thermal reaction. Mass spectrometry data (Fig. 14) can be interpreted as emission of triheptylamine (m/z = 311) and diheptyldisulfide (m/z = 262), which suggest that the thermal decomposition reaction can be formulated as for the previous precursors.

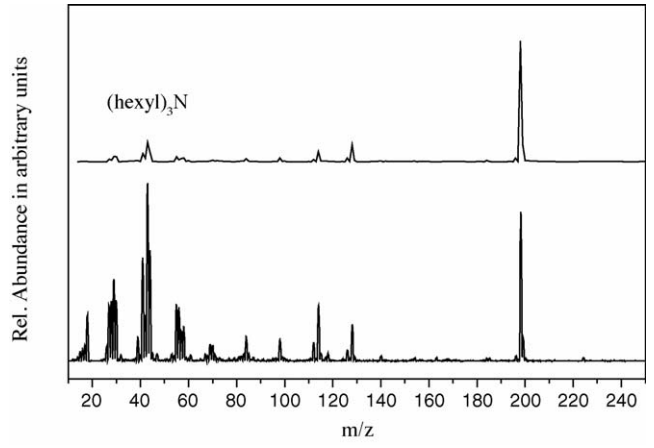

Fig. 12. Mass spectrum of $[(hexyl)_4N]_2[MoS_4]$ decomposition at 241 °C. *Note*: the top trace was taken from http://webbook.nist.gov/chemistry.

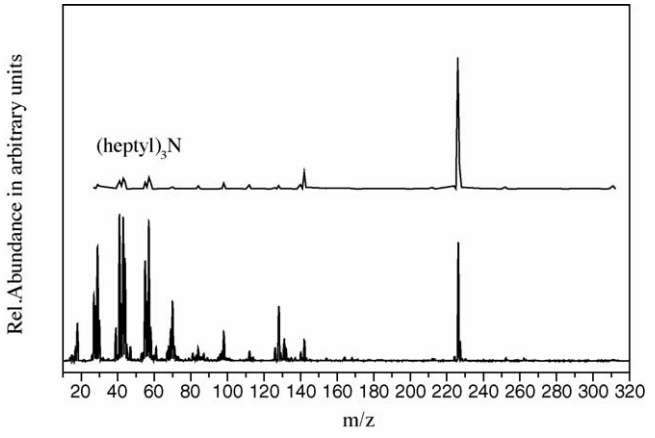

Fig. 14. Mass spectrum of $[(heptyl)_4N]_2[MoS_4]$ decomposition at 265 °C. *Note*: the top trace was taken from http://webbook.nist.gov/chemistry.

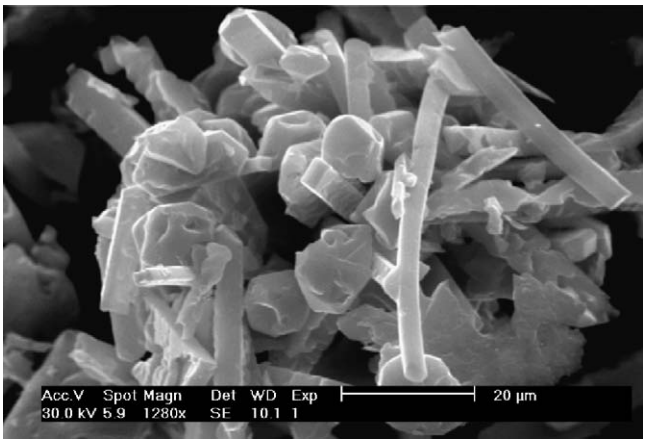

Fig. 15. SEM image of the thermal decomposition product from $[(methyl)_4N]_2[MoS_4]$.

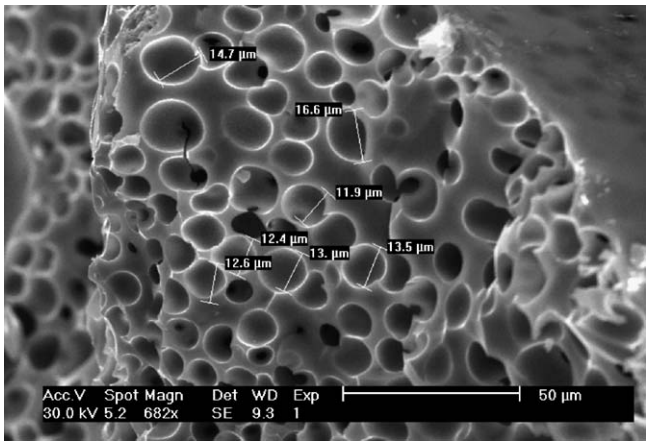

Fig. 17. SEM image of thermal decomposition product from $[(hexyl)_4N]_2[MoS_4]$.

3.3. Scanning electron microscopy

The morphology of the MoS_2 catalysts obtained by the thermal decomposition reactions of tetra-alkyl thiomolybdates was studied with SEM and images of selected materials are shown in Figs. 15–17. In general, formation of cavities (macropores) was observed for all samples and the morphology of the products changed gradually as a function of the alkyl precursor. The size of the cavities increases with the size of the alkyl group in the precursors. All samples exhibit a glassy appearance in SEM micrographs although they contained a high volume of micropores, as it was previously shown by nitrogen adsorption [8]. Such appearance is attributed to the presence of carbon in MoS_2, which is very good for transmission of electrons producing very high contrast images. The SEM micrograph of the tetramethylammonium precursor (Fig. 15) shows long faceted particles, similar to those observed for MoS_2 derived from ATM. Hence, the decomposition process of C1ATM is suggested to be topotactic (same morphology of precursor is maintained) as the process reported for ATM decomposition [39].

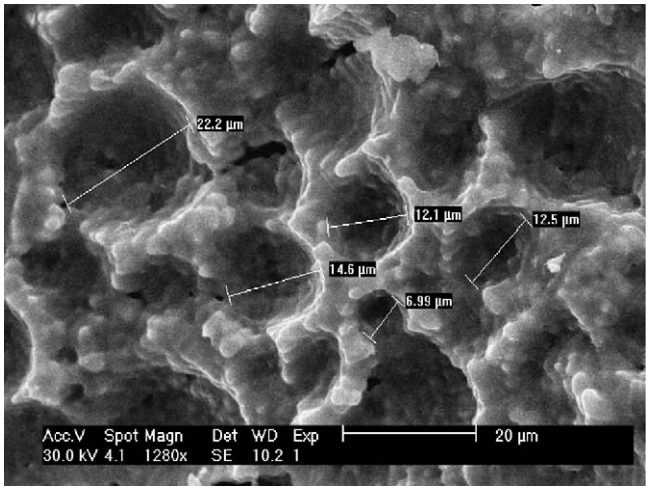

Fig. 16. SEM image of the thermal decomposition product from $[(propyl)_4N]_2[MoS_4]$.

In the SEM micrograph of the tetraethylammonium sample small cavities (about 2 and 6 μm) and large tunnels in the bulk of MoS_2 are seen. The process leading to the formation of cavities was suggested to be associated with the elimination of alkyl groups from the precursor [8]. In the SEM micrograph of tetrapropylammonium precursor (Fig. 16) an increased amount of cavities with a spherical form is observed. The size of these voids is in the range from about 6 up to 22 μm. The MoS_2 material surrounding the holes looks as agglomerated particles. In the SEM micrograph of the tetrabutylammonium thiomolybdate precursor a high density of cavities with a wide range of diameters (2–50 μm) are seen forming a spongy material. Small holes formed inside large cavities indicate that connectivity was developed in this MoS_2 catalyst. Using higher magnifications it is obvious that spherical bubbles have been formed during the decomposition process being responsible for this spongy morphology. The SEM pictures of the tetrapentylammonium and the tetrahexylammonium precursor (Fig. 20) show that the density of cavities is much larger compared to other precursors. In addition, the size distribution looks more homogeneous for these samples than for the others, particularly for the hexyl material. The SEM pictures of the tetraheptylammonium precursor reveal that it contains the largest cavities of all samples indicating that the size of alkyl group is responsible for cavity formation.

The (R_4N) compounds are well known for their applications as template molecules during the synthesis of zeolites and mesoporous materials [40]. The templates stabilise voids inside the solid structure of the precursor and these voids are proportional to the size of the alkyl group in the molecule. The MoS_2 materials generated from the tetra-alkylthiomolybdate precursors have been considered as amorphous mesoporous materials [41] or amorphous zeolites [42].

3.4. DSC experiments and X-ray powder diffraction

As pointed out above several compounds exhibit thermal events at relatively low temperatures that were not accompanied by weight changes. For a better understanding of the thermal properties DSC measurements were performed (Fig. 18) and

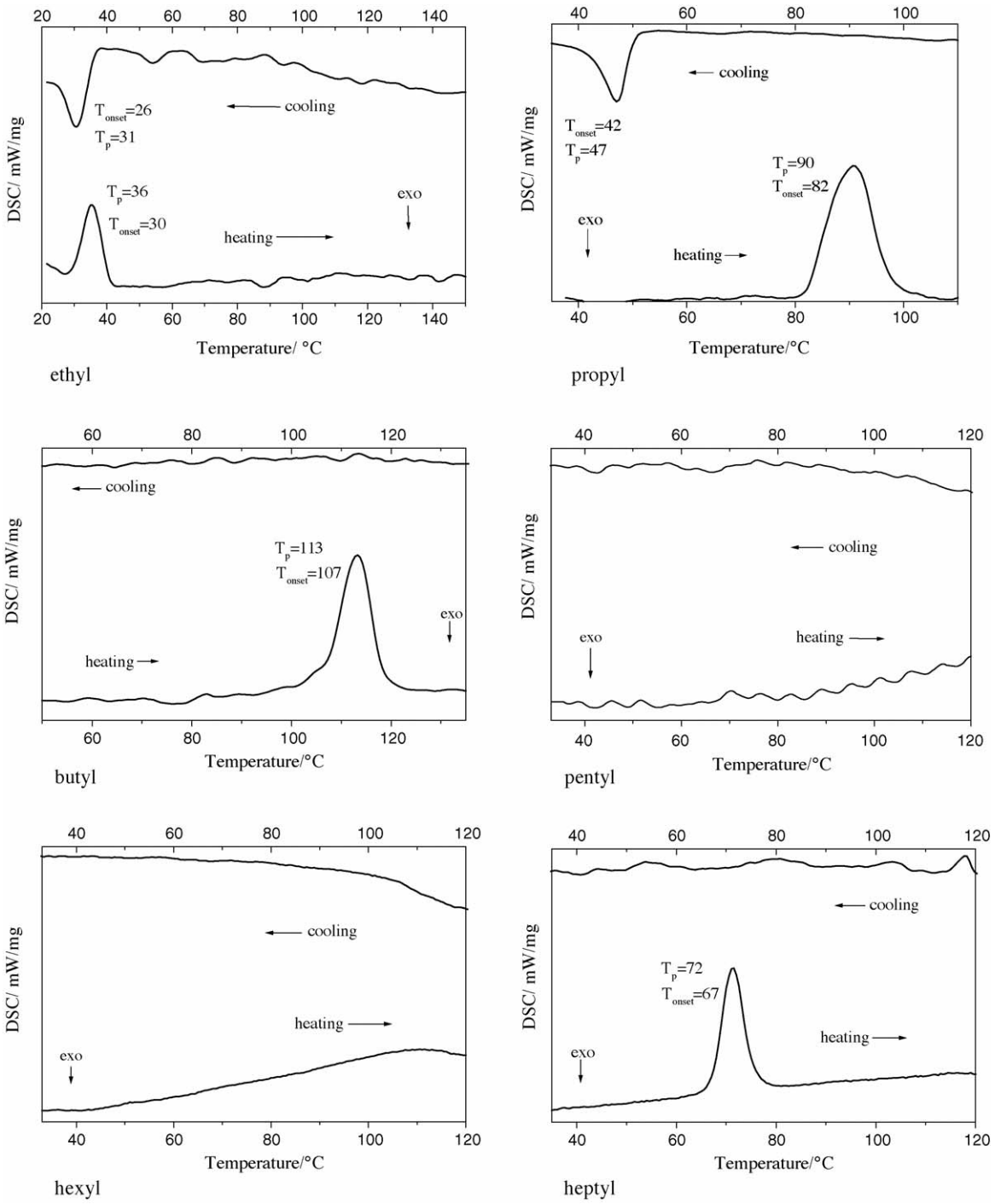

Fig. 18. DSC curves for the tetra-alkylammonium tetrathiomolybdate compounds.

the products were characterised with X-ray powder diffractometry (XPD). For several compounds in situ X-ray diffraction experiments were also performed.

For R = ethyl, events occur at very low temperatures, an endothermic event at T_{onset} = 30 °C in the heating curve and an exothermic peak at T_{onset} = 26 °C in the cooling curve. The XPD pattern taken after cycling through these thermal events reveals that the reflections are at the same positions as for the genuine material, but the profiles indicate a poorer crystallinity. The in situ X-ray experiment clearly show the occurrence of a new phase (Fig. 19) indicating that the phase transition was at least partially reversible. The signal in the DSC curve is intense suggesting that the transition may be first order however the exact order cannot be determined with this experiment.

The DSC trace of R = propyl displays an intense endothermic signal at T_{onset} = 82 °C in the heating curve and an exothermic peak at T_{onset} = 42 °C during the cooling ramp. The powder pattern after the heat treatment is different compared to the starting material indicating a structural phase transition. The in situ X-ray experiments (Fig. 20) clearly demonstrate that the

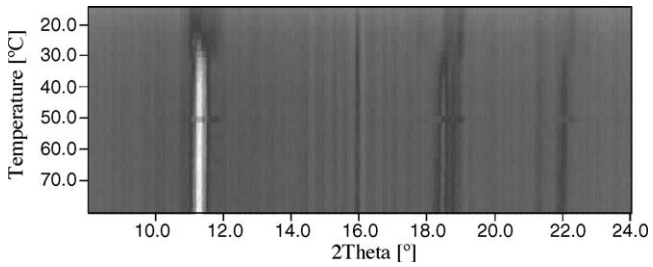

Fig. 19. Powder pattern of the in situ X-ray diffraction experiments for $((CH_3CH_2)_4N)_2MoS_4$.

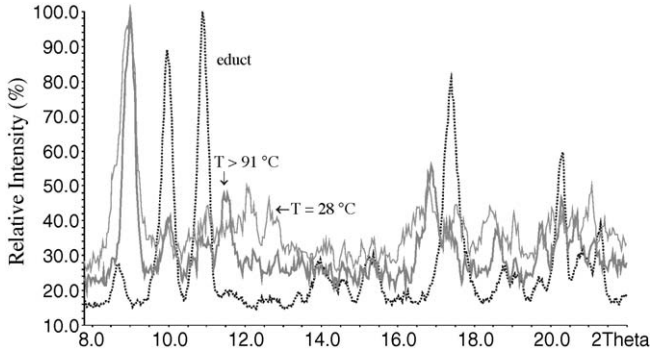

Fig. 20. Selected X-ray powder patterns of the in situ experiments performed for the tetrapropyl compound. Traces are: starting material, data collected at $T > 91\,^{\circ}C$ and after cooling to 28 °C.

starting material is first converted to a phase II, which in turn is transformed into a phase III during the cooling process. The reflections of phase II appear again heating phase III above 100 °C. A process of five cycles was performed with DSC, and in the heating cycles an endothermic event occurs always at about 90 °C and an exothermic peak was seen at about 40 °C in the cooling ramp. The structures of the three phases are closely related as evidenced by the similar X-ray powder patterns.

The R = butyl compound shows only one event during the heating cycle ($T_{onset} = 107\,^{\circ}C$), but no signal occurs during the cooling cycle. The X-ray powder pattern (Fig. 21) show strong reflections at positions different from that of the pristine material indicating that a new compound was formed with no reversibility to the original phase. The DSC curves of the tetrapentyl and tetrahexyl compounds display no pronounced signals up to

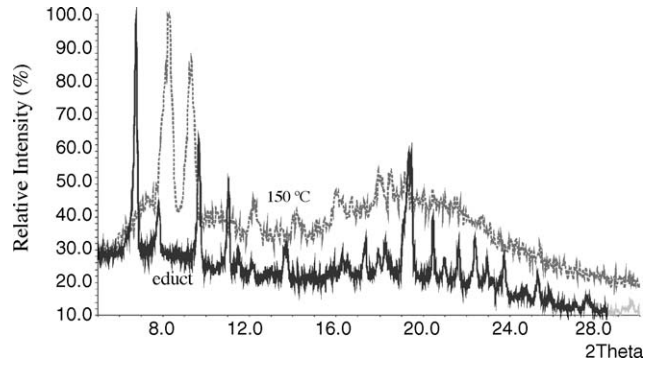

Fig. 21. Powder patterns of tetrabutylammonium tetrathiomolybdate before and after the DSC experiment. *Note*: the sample was heated to 150 °C.

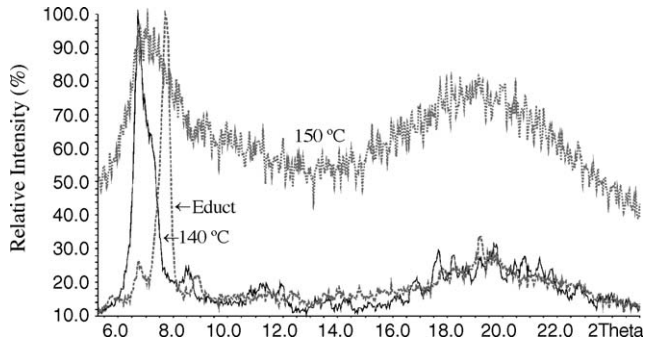

Fig. 22. Powder patterns for tetrapentyl tetrathiomolybdate. The displayed patterns are the starting material, after heating to 140 °C and after a treatment at 150 °C.

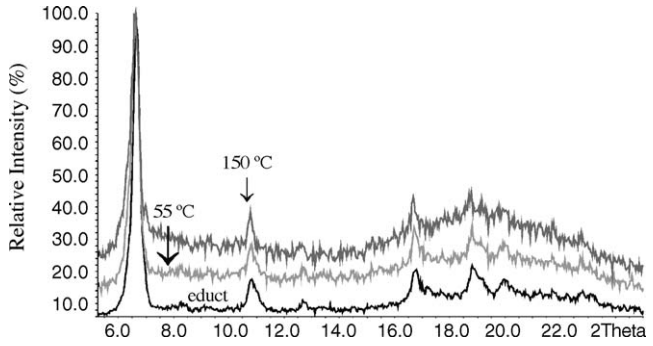

Fig. 23. Experiments of X-ray diffraction for tetrahexyl tetrathiomolybdate. Patterns were recorded from the starting material, after heating to 55 °C and after a treatment at 150 °C.

150 °C, but the traces are typical for glass-like transitions. When the experiment with R = pentyl was stopped at 140 °C the resulting material look like a melt and in the resulting powder pattern (Fig. 22) a strong and broad reflection is located at a different position compared with the starting material. When the compound is heated up to 150 °C the powder pattern of the product show only broad modulations of the background suggesting that the sample was destroyed. For the tetrahexyl sample no signal up to 150 °C is detected in the DSC curve and only a drift of the base line occurs. In the powder patterns (Fig. 23) taken after heating the material to 55 and 150 °C no differences are seen compared with the pristine material suggesting that the compound is stable up to 150 °C, being quite remarkable for this type of materials.

A different behavior is observed for R = heptyl. In the DSC curve an intense signal is seen at $T_{onset} = 67\,^{\circ}C$ in the heating curve, but no peak occurs in the cooling curve. The powder pattern of a sample heated to 80 °C (Fig. 24) shows only minor differences compared with the original sample. When the temperature is increased to 150 °C the sample decomposes and the powder diagram indicates the presence of a new compound. In situ X-ray diffraction experiments demonstrate that the sample melts at above 70 °C.

4. Discussion

The decomposition of tetra-alkyl thiomolybdates (methyl up to heptyl) shows different steps of weight loss involving differ-

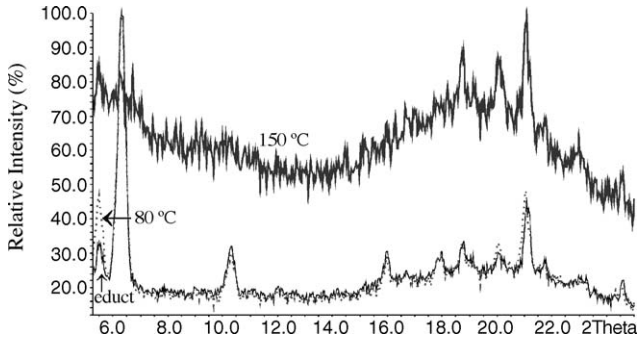

Fig. 24. Results of X-ray diffraction experiments for tetraheptyl tetrathiomolybdate. Patterns were recorded from the starting material, after heating to 80 °C and after a treatment at 150 °C.

ent energy processes as phase transitions, bond breaking and product elimination. Nevertheless, all precursors emit the same type of products during the thermal reaction, trialkylamines and dialkyldisulfides, indicating that besides the increasing complexity of the structure and composition of the precursors the reaction steps may be similar. The transformation of the tetralkylammonium cation R_4N^+ into two trialkylamine molecules and two alkyl radicals which react with two sulfur atoms of the MoS_4^{2-} anion seems to be the best scheme for the decomposition process. As shown above, the reaction process for all precursors can be represented with the general formula:

$$(R_4N)_2MoS_4 \rightarrow 2R_3N + R_2S_2 + MoS_2C_xN_yH_z$$

One possible explanation for the decomposition reaction may base on a concerted S_{N2} mechanism where the nucleophilic attack from one sulfur atom of the thiomolybdate anion to the α-carbon atom of R_4N^+ ions gives the trialkylamines as a product and also the dialkyldisulfides. With this mechanism there is only one transition state, i.e. a pentavalent C atom, usual in S_{N2} mechanisms.

For the two precursors with the largest tetraalkyl groups the sulfur content in the decomposition product is low indicating that the thermal reaction is more complex.

The composition of MoS_2 formed from the alkylthiomolybdates is a function of the precursor, the residual quantities of hydrogen and carbon in the final solid increase with the size of the alkyl group in the starting material, and for R = hexyl and heptyl the contamination with C and H is larger than the sulfur content. The materials formed from educts with R = methyl to pentyl contain sulfur in a Mo:S ratio of 1:2, i.e. they are stoichiometric. However, for the hexyl and heptyl groups the final materials contain less than the stoichiometric sulfur suggesting that carbon and hydrogen may be incorporated into the solid.

The low temperature thermal events were studied with DSC experiments in combination with in situ X-ray diffraction and the results highlight the complex thermal behavior of the materials. The sample with R = ethyl shows a partially reversible phase transition at a very low temperature of about 30 °C as evidenced by in situ XPD experiments. For R = propyl three different structural phases are identified with the in situ XPD investigations. The original material is first transformed to a phase II at about 90 °C. Obviously, such a low temperature indicates that only very small structural rearrangements can occur. Cooling the material down to room temperature an exothermic signal at $T_{onset} = 42$ °C indicates another structural rearrangement. The X-ray powder patterns recorded under in situ conditions clearly show the formation of a phase III, and all three structures must be very similar due to the similar X-ray powder patterns. The butyl compound irreversibly transforms at about 113 °C into a new phase. The DSC traces for R = pentyl and hexyl suggest a glass-like phase transformation with no pronounced signal in the curves up to 150 °C. The X-ray powder patterns give evidences that the sample with R = pentyl is transformed into a new compound at $T < 150$ °C, and at $T = 150$ °C it is destroyed yielding a featureless powder diagram. Interestingly, the tetrahexyl containing material could be heated up to 150 °C without any significant changes of the X-ray powder patterns. It is quite remarkable that this is the most stable precursor of the whole series of tetra-alkylammonium thiomolybdates. Surprisingly, the DSC curve for the tetraheptyl compound shows an intense endothermic event at $T_{onset} = 67$ °C but no signal occurs in the cooling cycle. The X-ray powder pattern is very similar to that of the genuine material. Heating the material to 150 °C leads to a decomposition of the sample and X-ray scattering experiments indicate the formation of a new compound.

5. Summary

The decomposition pattern of tetra-alkylammonium thiomolybdates presents several common features as:

- Phase transitions prior to decomposition, either reversible or irreversible, depending on the tetra-alkylammonium thiomolybdate precursor.
- Endothermic peaks during decomposition attributable to structural rearrangements and elimination reactions.
- Formation of trialkylamine and dialkyldisulfide products following a very similar mechanism.
- Increase of carbon and nitrogen contamination in MoS_2 residuals after decomposition with increasing size of R_4N. Decrease of S content below the stoichiometric value for the hexyl and heptyl precursors.
- Formation of cavities in MoS_2 materials obtained by thermal decomposition of tetra-alkyl thiometallates. The size of cavities increases with the size of the alkyl group in the precursor.

The thermal stability and decomposition of all compounds is complex with no simple relation between the number of events, its temperature and its composition. The materials with R = methyl and ethyl decompose in one sharp step, meanwhile a two-step decomposition occur for R = propyl and butyl. For R = pentyl, hexyl and heptyl the strong endothermic signal associated with the decomposition process become gradually broader with increasing size of the tetraalkyl chain covering a large temperature range. The temperature for phase transitions increase with increasing number of C atoms for R = ethyl, propyl and butyl. The remaining three materials show a different behavior with a glass-like transition for R = pentyl and hexyl.

Acknowledgments

The authors thank C. Teske for fruitful discussions and appreciate the technical attendance of C. Ornelas from CIMAV, and the financial support from DGAPA, project No. IN1 19602-3. The financial support by the Deutsche Forschungsgemeinschaft DFG (project: BE 1653/11-2) is also gratefully acknowledged.

References

[1] A. Müller, Transition Metal Chemistry—Current Problems of General, Biological and Catalytical Relevances, Verlag Chemie, Weinheim, 1981.
[2] K.S. Liang, J. Bernholc, W.H. Pan, G.J. Hughes, E.I. Stiefel, Inorg. Chem. 26 (1987) 1422.
[3] A.W. Naumann, A.S. Behan, US Patent 4,243,554 (1981).
[4] T.A. Pecoraro, R.R. Chianelli, US Patent 4,528,089 (1985).
[5] R.R. Chianelli, J. Jacobson, US Patent 4,650,563 (1987).
[6] G. Alonso, M. Del Valle, J. Cruz, V. Petranovskii, A. Licea-Claverie, S. Fuentes, Catal. Today 43 (1998) 117.
[7] G. Alonso, V. Petranovskii, M. Del Valle, J. Cruz-Reyes, A. Licea-Claverie, S. Fuentes, Appl. Catal. A: Gen. 197 (2000) 87.
[8] G. Alonso, G. Berhault, A. Aguilar, V. Collins, C. Ornelas, S. Fuentes, R.R. Chianelli, J. Catal. 208 (2002) 359.
[9] G. Alonso, M.H. Siadati, G. Berhault, A. Aguilar, S. Fuentes, R.R. Chianelli, Appl. Catal. A: Gen. 263 (2004) 109.
[10] G. An, Y. Chai, H. Zhong, C. Zhang, C. Liu, Prepr. Am. Chem. Soc.: Div. Pet. Chem. 50 (3) (2005) 344.
[11] H. Farag, K. Sakanishi, M. Kouzu, A. Matsumura, Y. Sugimoto, I. Saito, Prepr. Am. Chem. Soc., Div. Fuel Chem. 48 (2) (2003) 504.
[12] B.R. Srinivasan, S.N. Dhuri, M. Poisot, C. Näther, W. Bensch, Z. Naturforsch. B 59 (2004) 1083.
[13] B.R. Srinivasan, S.N. Dhuri, M. Poisot, C. Näther, W. Bensch, Z. Anorg. Allg. Chem. 631 (2005) 1087.
[14] D. Liu, Y. Li, R. Zhao, C. Liu, Prepr. Am. Chem. Soc., Div. Pet. Chem. 50 (1) (2005) 128.
[15] I. Bezverkhy, P. Afanasiev, M. Lacroix, Inorg. Chem. 39 (2000) 5416.
[16] A. Leist, S. Stauf, S. Löken, E.W. Finckh, S. Lüdtke, K.K. Unger, W. Assenmacher, W. Mader, W. Tremel, J. Mater. Chem. 8 (1998) 241.
[17] J.H. Zhan, Z.D. Zhang, X.F. Qian, C. Wang, Y. Xie, Y.T. Qian, J. Solid State Chem. 141 (1998) 270.
[18] Ch. Calais, N. Matsubayashi, Ch. Geantet, Y. Yoshimura, H. Shimada, A. Nishijima, J. Catal. 174 (1998) 130.
[19] X. Che, R. Fan, Chem. Mater. 13 (2001) 802.
[20] H. Liao, Y. Wang, S. Zhang, Y. Qian, Chem. Mater. 13 (2001) 6.
[21] M.M. Mdleleni, T. Hyeon, K.S. Suslick, J. Am. Chem. Soc. 120 (1998) 6189.
[22] R.R. Chianelli, Catal. Rev. Sci. Eng. 26 (1984) 361.
[23] A. Müller, A. Diemann, H.H. Heinsen, Chem. Ber. 104 (1971) 975.
[24] A. Müller, W. Hellmann, J. Schneider, U. Schimanski, U. Demmer, A. Trautwein, U. Bender, Inorg. Chim. Acta 65 (1982) L41.
[25] W. Eltzner, M. Breysse, M. Lacroix, M. Vrinat, Polyhedron 5 (1985) 203.
[26] F. Pedraza, S. Fuentes, Catal. Lett. 65 (2000) 107.
[27] T.P. Prasad, E. Diemann, A. Müller, J. Inorg. Nucl. Chem. 35 (1973) 1895.
[28] J. Brito, M. Ilija, P. Hernandez, Thermochim. Acta 256 (1995) 325.
[29] R.I. Walton, A.J. Dent, S.J. Hibble, Chem. Mater. 10 (1998) 3737.
[30] H.W. Wang, P. Skeldon, G.E. Thompson, G.C. Wood, J. Mater. Sci. 32 (1997) 497.
[31] R.I. Walton, S.J. Hibble, J. Mater. Chem. 9 (1999) 1347.
[32] G. Alonso, M. del Valle, J. Cruz, V. Petranovskii, A. Licea-Claverie, S. Fuentes, Catal. Today 43 (1998) 117.
[33] J.W. McDonald, G. Delbert Friesen, L.D. Rosenhein, W.E. Newton, Inorg. Chim. Acta 72 (1983) 205.
[34] G. Alonso, G. Aguirre, I.A. Rivero, S. Fuentes, Inorg. Chim. Acta 274 (1998) 108.
[35] O. Weisser, S. Landa, Sulfide Catalysts: Their Properties and Applications, Pergamon Press, Oxford, 1973.
[36] E. Rode, B. Lebedev, Zh. Neorg. Khim. 6 (1961) 1189.
[37] E. Diemman, A. Müller, Coord. Chem. Rev. 10 (1973) 79.
[38] G. Alonso, M. Del Valle, J. Cruz, A. Licea-Claverie, V. Petranovskii, S. Fuentes, Catal. Lett. 52 (1998) 55.
[39] E. Frommel, J. Diehl, J. Tamiglia, S. Pollack, Proceedings of the 12th North American Meeting of the Catalysis Society, Lexington, KY, 1991, p. PD-38.
[40] K. Holmberg, J. Colloid. Interf. Sci. 274 (2004) 355.
[41] G. Alonso, G. Berhault, F. Paraguay, E. Rivera, S. Fuentes, R.R. Chianelli, Mater. Res. Bull. 38 (2003) 1045.
[42] G. Alonso, M.H. Siadati, R.R. Chianelli, US patent 20050032636 (2005).